HHS Public Access

Author manuscript

Adv Healthc Mater. Author manuscript; available in PMC 2021 June 24.

Published in final edited form as:

Adv Healthc Mater. 2021 May ; 10(10): e2100315. doi:10.1002/adhm.202100315.

Stabilization of Damaged Articular Cartilage with Hydrogel-Mediated Reinforcement and Sealing

Jay M. Patel,
McKay Orthopaedic Research Laboratory, Department of Orthopaedic Surgery, University of Pennsylvania, 3450 Hamilton Walk, 371 Stemmler Hall, Philadelphia, PA 19104, USA; Translational Musculoskeletal Research Center, Corporal Michael J Crescenz VA Medical Center, 3900 Woodland Avenue, Philadelphia, PA 19104, USA; Department of Orthopaedics, Emory University School of Medicine, 201 Dowman Drive, Atlanta, GA 30322, USA

Claudia Loebel,
Translational Musculoskeletal Research Center, Corporal Michael J Crescenz VA Medical Center, 3900 Woodland Avenue, Philadelphia, PA 19104, USA; Department of Bioengineering, University of Pennsylvania, 210 South 33rd Street, Suite 240 Skirkanich Hall, Philadelphia, PA 19104-6321, USA

Kamiel S. Saleh,
McKay Orthopaedic Research Laboratory, Department of Orthopaedic Surgery, University of Pennsylvania, 3450 Hamilton Walk, 371 Stemmler Hall, Philadelphia, PA 19104, USA; Translational Musculoskeletal Research Center, Corporal Michael J Crescenz VA Medical Center, 3900 Woodland Avenue, Philadelphia, PA 19104, USA

Brian C. Wise,
McKay Orthopaedic Research Laboratory, Department of Orthopaedic Surgery, University of Pennsylvania, 3450 Hamilton Walk, 371 Stemmler Hall, Philadelphia, PA 19104, USA

Edward D. Bonnevie,
McKay Orthopaedic Research Laboratory, Department of Orthopaedic Surgery, University of Pennsylvania, 3450 Hamilton Walk, 371 Stemmler Hall, Philadelphia, PA 19104, USA; Translational Musculoskeletal Research Center, Corporal Michael J Crescenz VA Medical Center, 3900 Woodland Avenue, Philadelphia, PA 19104, USA

Liane M. Miller,
McKay Orthopaedic Research Laboratory, Department of Orthopaedic Surgery, University of Pennsylvania, 3450 Hamilton Walk, 371 Stemmler Hall, Philadelphia, PA 19104, USA

James L. Carey,
McKay Orthopaedic Research Laboratory, Department of Orthopaedic Surgery, University of Pennsylvania, 3450 Hamilton Walk, 371 Stemmler Hall, Philadelphia, PA 19104, USA

lemauck@pennmedicine.upenn.edu.

Conflict of Interest

J.M.P., C.L., J.A.B., and R.L.M. are inventors on a PCT patent application (PCT/US2019/041623) regarding this technology.

Supporting Information

Supporting Information is available from the Wiley Online Library or from the author.

Jason A. Burdick,
McKay Orthopaedic Research Laboratory, Department of Orthopaedic Surgery, University of Pennsylvania, 3450 Hamilton Walk, 371 Stemmler Hall, Philadelphia, PA 19104, USA; Translational Musculoskeletal Research Center, Corporal Michael J Crescenz VA Medical Center, 3900 Woodland Avenue, Philadelphia, PA 19104, USA; Department of Bioengineering, University of Pennsylvania, 210 South 33rd Street, Suite 240 Skirkanich Hall, Philadelphia, PA 19104-6321, USA

Robert L. Mauck
McKay Orthopaedic Research Laboratory, Department of Orthopaedic Surgery, University of Pennsylvania, 3450 Hamilton Walk, 371 Stemmler Hall, Philadelphia, PA 19104, USA; Translational Musculoskeletal Research Center, Corporal Michael J Crescenz VA Medical Center, 3900 Woodland Avenue, Philadelphia, PA 19104, USA; Department of Bioengineering, University of Pennsylvania, 210 South 33rd Street, Suite 240 Skirkanich Hall, Philadelphia, PA 19104-6321, USA

Abstract

Cartilage injuries and subsequent tissue deterioration impact millions of patients. Since the regeneration of functional hyaline cartilage remains elusive, methods to stabilize the remaining tissue, and prevent further deterioration, would be of significant clinical utility and prolong joint function. Finite element modeling shows that fortification of the degenerate cartilage (Reinforcement) and reestablishment of a superficial zone (Sealing) are both required to restore fluid pressurization within the tissue and restrict fluid flow and matrix loss from the defect surface. Here, a hyaluronic acid (HA) hydrogel system is designed to both interdigitate with and promote the sealing of the degenerated cartilage. Interdigitating fortification restores both bulk and local pericellular tissue mechanics, reestablishing the homeostatic mechanotransduction of endogenous chondrocytes within the tissue. This HA therapy is further functionalized to present chemo mechanical cues that improve the attachment and direct the response of mesenchymal stem/stromal cells at the defect site, guiding localized extracellular matrix deposition to “seal” the defect. Together, these results support the therapeutic potential, across cell and tissue length scales, of an innovative hydrogel therapy for the treatment of damaged cartilage.

Keywords

biomechanics; cartilage; hydrogels; mechanobiology; mesenchymal stem cells

1. Introduction

Articular cartilage is a remarkably durable tissue that enables load transmission and joint articulation.[1] The dense extracellular matrix (ECM) and high proteoglycan (PG) content of the tissue promote fluid pressurization,[2,3] a characteristic critical for resisting the complex stresses in joints.[4] Focal cartilage injuries introduce new free surfaces that allow fluid to flow more easily from the tissue,[5] reducing its ability to support loads. Such injuries can lead to a progression of cell death and matrix catabolism and loss that propagate from a focal defect.[6,7] Coupled with chemo-enzymatic degradation by matrix proteases,[6,8,9] the

tissue adjacent to defects is highly susceptible to matrix depletions,[10,11] exacerbating the decrease in fluid pressurization capacity. This degenerated tissue is more vulnerable to wear, [12] initiating a vicious cycle that increases defect size and concludes in joint-wide osteoarthritis (OA). The development of a therapeutic to delay, or even prevent, this deterioration could alter disease progression in millions of patients, forestalling the need for joint replacement.[13]

Current treatments for articular lesions include chondroplasty (removal), microfracture (marrow stimulation), mosaicplasty (grafting), and chondrocyte implantation.[14] These procedures result in short-term symptom relief, but long-term outcomes are inconsistent or ineffective,[15,16] due in part to the formation of mechanically inferior repair tissue or disregard for the surrounding cartilage tissue.[14] Thus, since new hyaline cartilage does not form with these approaches, techniques to preserve the remaining articular cartilage may be of clinical importance, preventing further wear and OA progression and delaying the need for total joint replacement.

To counter the detrimental biomechanical consequences experienced during cartilage injury and erosion, several groups have used biomaterials or chemical crosslinking methods in an attempt to fortify or protect the tissue. Application of hyaluronic acid (HA)[11] or poly(ethylene glycol)[17] improves tissue biphasic mechanical properties. However, the response of endogenous chondrocytes to these treatments, beyond viability measurement, has not been explored. Alternatively, crosslinking the cartilage matrix, for example with genipin,[18] can improve biomechanics and wear properties. However, the concentrations necessary for fortification may be cytotoxic to endogenous chondrocytes. Thus, while encouraging and motivating for the current study, cartilage protection strategies do not simultaneously fortify and seal the articular cartilage, and so additional design and development is needed for clinical implementation.

Beyond cartilage salvage and fortification, intra-articular injection of orthobiologics has become increasingly popular in sports medicine, especially for nonsurgical palliative care. These include injection of platelet-rich plasma (PRP), bone marrow aspirate concentrate (BMAC), and, perhaps most commonly, mesenchymal stem/stromal cells (MSCs).[19] MSCs have long been utilized in tissue engineering and therapeutic applications in orthopedics, due in part to their multilineage, regenerative potential. Furthermore, MSC phenotype and function can be dictated by the microenvironment through biological, chemical, and physical cues.[19-21] However, in the clinical setting, while some anecdotal evidence exists of improvement in patient-reported outcomes following MSC injection into joints,[22,23] the localization and behavior of these progenitor cells postinjection are generally uncontrolled. [24] Beneficial effects of MSC injections have been attributed to immunomodulation and/or cartilage regeneration, though these results are inconsistent and require further validation and assessment.[14] To date, it has not been demonstrated that these injected therapeutic cells participate in sealing the defect.

Here, we coupled biomaterial augmentation and MSC interactions to stabilize damaged cartilage in an effort to prevent further deterioration. Specifically, we developed an HA therapy to modify the damaged cartilage surface and confirmed its ability to form an

integrated microenvironment with, and improve biphasic mechanics of, the cartilage at the injury site. HA therapy of degenerated cartilage explants also restored chondrocyte mechanotransduction to near-healthy levels, indicating the protective effect of this approach. Next, using both the improved micromechanics at the damaged cartilage interface and cell-adhesive ligands conjugated to the HA therapy, we improved MSC attachment to the injury site and programmed their mechanosensation to generate a promatrix synthesis phenotype, leading to the deposition of robust extracellular matrix to "seal" injured cartilage. Taken together, these results detail the development of a novel therapeutic strategy to restore cartilage biomechanics and to potentially prevent subsequent wear and degeneration.

2. Results and Discussion

2.1 Reinforcement and Sealing Are Required to Restore Cartilage Biomechanics

Injury to articular cartilage and subsequent arthritic degeneration lead to compromised joint function (Figure 1A). A hallmark of disease is the reduction of PG and collagen at the damaged surface,[25] resulting in progressive worsening of both macro- and microscale poroelastic mechanics.[12,26] Chondrocytes regulate their biosynthetic activities in response to chemo-mechanical cues derived from the extracellular matrix and joint loading, and are negatively impacted by these degenerative changes.[27,28] This renders both cells and ECM susceptible to continued deterioration. To combat the physical effects of this degeneration, two potential preservative options have been explored and are of interest (Figure 1B): reinforcing the damaged cartilage matrix[17,18] or sealing the tissue by adding a low-permeability layer at its surface.[11,29]

To better understand how such potential treatment modalities (reinforcement and sealing) influence cartilage biomechanics, we utilized finite element modeling to predict patterns of fluid flow and pressurization (Figure S1, Supporting Information) in the context of cartilage injury. Physiologic strain (10%;[30,31]) imposed by a spherical indenter in a simulated degenerated defect (removal of the superficial zone [SZ], modulus/permeability from subsequent testing) increases fluid flow both in deeper layers of cartilage as well as at the surface (Figure 1C,D). Interestingly, fortification of this degenerated cartilage (Reinforced) partially restored fluid pressurization and fluid flow in the lower layers of cartilage, but did not attenuate the higher flow velocities at the surface (Figure 1C,E, Figure S1, Supporting Information). To reduce fluid flow at this surface, and potentially reduce the convection-mediated loss of matrix elements at this tissue boundary, a layer of tissue resembling the superficial zone (SZ) of cartilage was required in the model. These results mimic the findings of Owen and Wayne which showed, via finite element modeling, that a "surface layer" over repair cartilage tissue could reduce fluid flow at the cartilage surface.[29] Finally, simulated reinforcement of the degenerated matrix, combined with sealing with an SZ-like layer of tissue over the defect, restored fluid flow both below and at the surface. This suggests that functional restoration of degenerated defects will require both internal reinforcement (to restore both functional biomechanics and chondrocyte mechanotransduction) as well as modifications that promote the formation of a superficial-zone-like layer to reduce fluid and matrix flow from the damaged cartilage boundary.

2.2 Hyaluronic Acid-Based Therapy Designed to Reinforce and Seal Damaged Cartilage

Because a combination of fortifying and sealing may restore native function, we designed and developed a biomaterial-mediated approach to modify the damaged cartilage interface. This strategy's first objective was to reinforce the damaged cartilage (Figure 2A), improve multiscale mechanics, and restore chondrocyte behavior within the existing cartilage tissue. We then utilized this new microenvironment to improve the adhesion and mechano-sensation of mesenchymal stem cells on the defect surface, with the goal of guiding these cells towards a pro-matrix synthesis phenotype for the deposition of fibrous matrix to "seal" defects (Figure 2B).

Our approach centered on HA, a biomolecule present in synovial fluid and native cartilage matrix that is commonly used in viscosupplementation therapies for damaged knee joints.[32] HA is modifiable to tune its functional attributes.[33,34] Here, modified HA (sodium hyaluronate, ≈75 kDa premodification, ≈25 kDa postmodification) via oxidation (11.4% substitution), methacrylation (32% modification), and peptide conjugation to add functionality to the HA (Figure 2C, Figure S2, Supporting Information). Oxidation of the HA backbone results in conversion of adjacent hydroxyl groups into aldehyde groups, which can subsequently form dynamic covalent crosslinks with free amines in cartilage tissue via Schiff-base reaction.[35] Methacrylation of HA allows for crosslinking and gelation via light-induced photopolymerization, as well as peptide conjugation via a Michael addition reaction between the methacrylates and thiols on the peptides. For this work, aldehyde-substituted HA was methacrylated (MeHA-ALD; HA therapy) and conjugated with fluorescent peptides (fluorescein. This modified HA was attached to exposed cartilage; attachment was significantly attenuated when aldehydes in the material were prequenched with *tert*-butyl-carbazate (Figure S3, Supporting Information). The duration of exposure also regulated attachment, with longer times of application resulting in increased fluorescent intensity on cartilage plugs, likely due to increased time for interactions with free amines in the tissue (Figure S4, Supporting Information), all while maintaining cytocompatibility (Figure S5, Supporting Information). These results indicate the ability of aldehyde functionalization to improve the adherence of the HA therapy to cartilage tissue.

To generate a stable interdigitating microenvironment, HA therapy solution (4 wt%) was applied to a cartilage defect, allowed to diffuse into and integrate with the tissue, and was photocrosslinked with UV light for 10 min (320–400 nm, 5 mW cm^{-2}) (Figure 2D). From an axial view, the HA therapy appeared to contour to the surface of the defect even after extensive washing (Figure S6, Supporting Information). Upon further investigation of tissue cross-sections, it was evident that, within 1 min of application, the HA therapy had in fact diffused into the cartilage tissue, and was crosslinked in place, forming an interdigitated cartilage-HA layer approximately 150 μm thick (Figure 2E). Increasing the time of application (1, 5, 10 min) prior to UV light exposure resulted in an increased infiltration depth (150–250 μm) but reduced fluorescent intensity (Figure S7, Supporting Information), likely due to time allowing the HA solution to diffuse further into the cartilage. Notably, this interdigitated layer did not extend beyond the topmost 150–250 μm of the tissue, likely due to the reduction of UV-light irradiance as an exponential decay function of cartilage depth (Figure S8, Supporting Information), with irradiance being halved by 200–300 μm below the

cartilage surface (τ = 119.1 μm). Thus, rather than forming a coating over the damaged surface that would be susceptible to delamination, we found that the HA therapy interdigitates with the cartilage.

2.3 Interdigitating HA Enhances Cartilage Tissue Mechanics and Is Stable Both In Vitro and In Vivo

Previous studies have reported cartilage fortification at the macroscale after genipin crosslinking,[18] cartilage surface modification,[11] and with the introduction of interpenetrating polymer networks.[17] To determine the functional consequence of our interdigitated HA therapy, we assessed tissue mechanics across length scales (Figure 3A). We evaluated either fresh focal defects (FD; surface layer removed only) or focal defects that had progressed in their degeneration (degenerated defects (DD); surface layer removed, collagenase digested), with macroscale properties evaluated via indentation testing. Results from this assay showed little effect of the HA therapy on FD tissue (Figure S9, Supporting Information), but a significant increase in compressive modulus and decrease in permeability with HA therapy applied to DD tissue (Figure 3B,C). Interestingly, nanoindentation at the cellular length scale (10 μm radius) revealed that the HA therapy significantly improved micromechanics for both focal and degenerated defects (Figure 3D, Figure S9, Supporting Information). To evaluate the persistence of the interdigitating HA, cartilage explants (with the superficial zone removed) were subject to HA application and crosslinking, serial saline rinses, and incubation at 37 °C for up to 7 d. Though 40% of measured fluorescence was lost after 1 d (due to the loss of the soluble fraction that did not crosslink), ≈60% of the HA therapy persisted through 7 d of incubation, indicating that the interdigitated biomaterial is retained and stable (Figure S10, Supporting Information). Finally, to evaluate the durability of the HA therapy in an in vivo setting, where load bearing and degradative enzymes in the synovial environment could accelerate loss, a study in Yucatan minipigs was performed. Partial thickness defects (4 mm diameter $x \approx 200$ μm deep) were created in the trochlea of each knee of three animals, followed by HA solution application and light-mediated photocrosslinking (Figure 3E). Light exposure for either 5 or 15 min resulted in the retention of fluorescent material at the defect site (Figure 3F,G) at 7 d postoperatively, demonstrating the in vivo feasibility of this approach in the joint environment.

2.4 Fortification of Degenerated Cartilage Restores Chondrocyte Mechanotransduction

The loss of matrix elements and mechanical integrity in the vicinity of a cartilage defect alters chondrocyte homeostasis, mechanotransduction, and phenotype,[27,36] and renders the tissue more susceptible to wear. Fortification of the micromechanics of the cartilage matrix (Figure 3D), inclusive of the pericellular matrix (PCM) that encases each chondrocyte (Figure 4A) may have a restorative effect on cell behavior. To test this hypothesis, cartilage explants were maintained for 18 d in either a control basal media or in a “degenerative media” (containing IL-1β), and then subjected to HA therapy (application and crosslinking; Figure S11, Supporting Information). Chondrocyte mechanotransduction was evaluated by assessing calcium signaling dynamics under isotonic conditions and immediately following a hypotonic osmotic challenge (Figure 4B); prior studies have shown that chondrocytes within degenerated tissue are more responsive to this challenge.[27,37] In degenerated cartilage, without fortification, osmotic challenge markedly increased the responsivity of

chondrocytes (Figure 4C,D). This is likely due to increased calcium flux through stretch-activated ion channels as a consequence of cell swelling against a weaker PCM.[38] Fortification with our HA therapy attenuated this response, restoring chondrocyte mechanotransduction to that observed in control healthy conditions. These findings were further validated in a 3D culture system. Chondrocytes in agarose were allowed to deposit pericellular matrix for 3 d and were then subjected to hypotonic swelling before or after interdigitating HA therapy. In this scenario, as in native tissue, fortification of the PCM restored the chondrocyte mechanoresponse to baseline (Figure S12, Supporting Information). These data support that fortification of the microenvironment via the interdigitating HA therapy can improve chondrocyte health and restores native mechanoresponsivity.

2.5 Reprogramming of the Tissue Surface Enhances MSC Adhesion and Mechanosensation

The above results demonstrate the potential of the interdigitating HA therapy to restore biphasic mechanics and mechanotransduction to a hypotonic challenge, yet this alone is unlikely to counter the increased flow at the surface of the defect (Figure 1C). To address the issue of fluid flow and matrix loss from the surface, we next targeted and modified the chemomechanical attributes of the interface. Specifically, we coupled our HA modification with an existing palliative treatment for osteoarthritis, MSC injections.[19] While there exists some promising data in terms of patient-reported outcomes following MSC injection,[39,40] the localization of these cells to the site of injury, and their response upon arrival, is very much uncontrolled (Figure 5A).[24] Moreover, degeneration reduces the ability of MSCs to adhere to the cartilage surface (Figure S13, Supporting Information). To improve MSC adhesion to the damaged cartilage surface and to control their response, we introduced new chemo-mechanical cues at this interface. Since cellular attachment to HA is mediated by surface presented CD44 or through interactions with aldehydes, both of which provide relatively weak adhesion, additional cell-adhesive cues were added to enhance the “sticky-ness” of the modified surface (Figure S14, Supporting Information, [41,42]). Specifically, we conjugated RGD peptides to the existing methacrylate groups (Figure 2C), to provide additional sites for MSC attachment.

To test whether this modification impacted MSC adhesion and mechano-sensation, thin devitalized cartilage discs (8 mm diameter × 100 μm) were sterilized, digested to mimic degeneration, subjected to biomaterial application and crosslinking, and seeded with MSCs. Focal adhesions were visualized via paxillin staining and morphology via F-actin staining. Application of the HA therapy presenting RGD resulted in increases in cell area and the area and number of focal adhesions per cell, with MSCs spreading directly on top of the cartilage-HA interdigitating network (Figure 5B). Cell area and adhesion area per cell increased by a factor of ≈2 (Figure 5C,D). Mechanosensing by cells adhered to this new chemo-mechanical interface was determined by analysis of the localization of Yes-activated protein 1 (YAP) and Transcriptional coactivator with PDZ-binding motif (TAZ).[20,43] With HA therapy (+RGD), these transcriptional coactivators translocated to the nucleus to a greater degree (Figure 5E,F). This increased nuclear localization has been reported to increase downstream transcription of genes related to cell proliferation and matrix synthesis.

[43] The relative impact of RGD and surface fortification on the adhesion and mechanoresponse of MSCs was also determined. Mechanical fortification alone (HA therapy without RGD) was sufficient to improve YAP/TAZ nuclear localization in degenerated defects, while HA therapy with RGD was required to enhance cell adhesion and mechanosensation of the underlying surface in fresh focal defects (FD; nondigested tissue) (Figures S15 and S16, Supporting Information). This is likely due to the higher degree of fortification in degenerated defects (Figure 3D). Of additional note, even in the absence of RGD peptide conjugated to the HA therapy, cells could adhere and spread on the cartilage surface. This finding supports that the HA therapy interdigitates with the native tissue (which provides for binding moieties) while the material stiffens the surface to which the cells are attached. Finally, we evaluated the tunable nature of the HA-modified interface by evaluating response as a function of light-mediated crosslinking time (0, 5, 15 min). Results showed step-wise increases in both adhesion area and nuclear levels of YAP/TAZ with the amount of crosslinking (Figures S17 and S18, Supporting Information), likely attributed to step-wise increases in the micromechanics (Figure S19, Supporting Information). Thus, these results indicate that the modified HA therapy can improve MSC adhesion to the cartilage defect surface and be tuned to regulate their perception of the surface mechanics.

2.6 HA Therapy Promotes Matrix Deposition and “Sealing” of Damaged Cartilage

Prior studies have indicated that the downstream impact of increased cell spreading and mechano-sensation (YAP/TAZ), is matrix formation and fibrosis.[44,45] Given that our goal was to limit fluid flow and matrix loss from the tissues, we sought to utilize the improved adhesion, spreading, and mechanosensation of MSCs on modified cartilage to direct rapid matrix deposition at the interface (Figure 6A). One marker of a promatrix synthesis phenotype is the incorporation of α-smooth muscle actin (α-SMA) into stress fibers.[46] After 1 week of culture, MSCs cultured on cartilage discs modified with HA therapy (+RGD) showed a significant increase in the portion of α-SMA fiber-positive cells compared to those on control cartilage without treatment (Figure 6B,C). Similar to our findings with YAP/TAZ (Figure S18, Supporting Information), we noted a stepwise increase in fraction of α-SMA positive stress fibers with increasing light exposure/crosslinking (0, 5, 15 min) duration, in both focal and degenerated defects (Figure S20, Supporting Information). To visualize this newly synthesized extracellular matrix (ECM) deposited by MSCs, we adapted a metabolic labeling technique that uses a functional analog of L-methionine called L-azidohomoalanine (AHA), which is incorporated by cells into nascent matrix proteins and stained via dye-conjugated cycloaddition.[47,48] A greater amount of matrix was deposited on cartilage modified with the interdigitating HA therapy (Figure 6D,E) after 7 d of culture, with nascent matrix clearly accumulating on the top surface of the reprogrammed microenvironment. This finding was confirmed in a cartilage explant model, where a dense, aligned, collagen- and fibronectin-rich layer of tissue formed at the cartilage surface, approximately 20 μm thick (Figure 6F, Figure S21, Supporting Information), with HA therapy. To account for and understand the impact of this newly formed fibrous layer, we updated our FE model to include a 20 μm layer of aligned tissue. Both the tensile properties and the permeability of this superficial tissue impact fluid flow, and flux at the surface can be reduced to near healthy values (Figure 6G). These results demonstrate the

ability of the HA therapy to enhance the adhesion and mechanobiology of the cells to produce a superficial layer of tissue to “seal” damaged cartilage and preserve tissue function.

3. Conclusion

We developed a biomaterial system that reprograms the damaged articular surface to stabilize and preserve existing tissue. In particular, we first showed that the HA therapy could attach to and interdigitate with damaged cartilage tissue, forming a stable tissue-biomaterial microenvironment with partially restored biphasic mechanical properties. Importantly, this fortification restored chondrocyte mechano-transduction to healthy behavior. To address fluid flux, and ultimately matrix loss, from the defect surface, we directed the attachment and activity of MSCs, a clinically relevant cell type that is commonly injected into knee joints for OA treatment. Using chemomechanical cues enabled by the interdigitated microenvironment, we improved cell attachment to degenerated tissue, which resulted in deposition of abundant nascent extracellular matrix that was aligned parallel to the articular surface, similar to healthy superficial cartilage. With this novel biomaterial design, and assessment of multi-scale biomechanics and mechanobiology, our data support a new technology that may reinforce and seal defects, restore biomechanics, direct MSC localization and sealant formation, and ultimately preserve cartilage function and prolong joint health after injury. Certainly, additional optimization of the system is required, including addressing potential UV exposure effects on chondrocytes within the matrix, which may be mitigated with alternative photo-initiators and light sources (e.g., ruthenium/sodium persulfate under visible light[49]). Additionally, the reinforcement of degenerated cartilage was modest, but consistent across samples. Further tuning of gel modification, concentration, and crosslinking may better enhance mechanics. Evaluation is also required in longer-term cartilage explants to more fully elucidate chondrocyte phenotypic rescue, stability of the material and sealant, and continued stabilization of the matrix, especially under cyclic fatigue loading. One limitation of the current work, as it relates to sealant formation, is that we allowed the tissue to develop under static culture conditions; the dynamic joint environment may present challenges to adhesion, and so fortification, cell adhesion, and layer formation will need to be investigated under dynamic conditions. Finally, subsequent studies in large-animal models will need to determine the efficacy and durability this reinforcement and sealing with respect to preventing cartilage deterioration, prior to translation and clinical use. These findings also serve as a basis to sealing other load-bearing tissues that would benefit from controlled and localized matrix fortification and ECM deposition.

4. Experimental Section

Finite Element Modeling:

Finite element modeling was performed in FEBio software.[50] A cartilage wedge model (10° wedge) was created with a cartilage thickness of 1mm, cartilage radius of 4mm, and indenter radius of 1 mm (Figure S1, Supporting Information). Boundary constraints were placed on the bottom cartilage surface (no x, y, z displacement), inner curve (no x, y displacement), outer surface (no x, y, z displacement), forward surface (no y displacement),

and back surface (symmetry against plane). A displacement of 200 μm was applied to the cartilage surface, and the resulting fluid flow was calculated. Cartilage was modeled as a biphasic neo-Hookean material with spherical fiber distribution.[51] Healthy cartilage properties (baseline) were set to a solid volume fraction of 0.2, modulus (E) of 2.233 MPa and permeability (k) of 0.000532 $mm^4\ N^{-1}\ s^{-1}$. Degenerate cartilage properties were created by changing values to E = 1.15 MPa and k = 0.001621 $mm^4\ N^{-1}\ s^{-1}$. Reinforced cartilage, indicative of cartilage with interpenetrating MeHA-ALD hydrogel, had properties set to E = 1.385 MPa and k = 0.001124 $mm^4\ N^{-1}\ s^{-1}$. Healthy, degenerated, and reinforced values were obtained via indentation testing (described below). Superficial zone (SZ; Sealed) cartilage was modeled as a 20 μm layer of tissue, considered biphasic neo-Hookean, reinforced with an orthotropic elastic material (parallel to surface: $E_1 = E_2$ = 85 MPa; perpendicular to surface: E_3 = 17 MPa), and permeability of 0.000265 $mm^4\ N^{-1}\ s^{-1}$ (half of underlying cartilage,[52]). Combinations of reinforcement and sealing were evaluated, and sealant layer properties (modulus and permeability) were varied to establish their effect on fluid flux (Figure 6G).

HA Therapy Synthesis and Characterization:

The modified hyaluronic acid (HA) for the HA therapy was synthesized in three consecutive steps: oxidation for aldehyde substitution, methacrylation, and peptide conjugation. First, sodium hyaluronate (75 kDa; LifeCore Biomedical) was dissolved in deionized water (DI H_2O) at 10 mg mL^{-1} (1 wt%) and oxidized with sodium periodate ($NaIO_4$; 5.35 mg mL^{-1}) for 3 h. The reaction was terminated by adding ethylene glycol (140 μL per 1 g HA), and the solution was dialyzed against DI H_2O with a 6000–8000 molecular weight cut-off (MWCO) dialysis membrane for 3 d (3 changes per day), frozen, and lyophilized to form dry HA-ALD. Next, HA-ALD was dissolved at 10 mg mL^{-1} (1 wt%) in DI H_2O and methacrylated by adding a 20-fold excess of methacrylic anhydride (target modification of 30%), and the reaction was maintained at pH 8.0–9.0 for 6 h at 4 °C. The reaction was terminated by stirring rigorously overnight causing the methacrylic anhydride to undergo hydrolysis,[53] followed by dialysis for 10 d, freezing, and lyophilization to yield dry MeHA-ALD. Finally, for peptide conjugation with either fluorescent (GCKKG-5,6 carboxyfluorescein; synthesized in house,[53]) or cell-adhesive (RGD peptide; GCGYGRGDSPG, Genscript RP20297,[47]) peptides, MeHA-ALD was dissolved at 2 mg mL^{-1} (0.2 wt%) in 0.2 M triethanolamine buffer (pH 8.0), and peptide was added to the solution (1.0 μmol per 40 mg MeHA-ALD; 1.0×10^{-3} M concentration in 4 wt% gel). The solution was reacted at 37 °C for 30 min, and then overnight at room temperature. Following dialysis for 7 d, the solution was frozen and lyophilized to yield a final product (FITC-MeHA-ALD or RGD-MeHA-ALD).

Aldehyde substitution was measured with a commercially available aldehyde quantification kit (Abcam; ab138882), which involved reaction of aldehydes with a fluorogenic dye (Figure S2, Supporting Information). Methacrylation degree was determined via nuclear magnetic resonance (^{1}H NMR; Bruker DMX 360 and 300 MHz spectrometer) (Figure S2, Supporting Information), by integration of the vinyl singlets (1H each) relative to the sugar ring of hyaluronic acid. Peptide conjugation of FITC was apparent in the fluorescent nature of the biomaterial, and conjugation of RGD was verified by the superior attachment of

MSCs on RGD-MeHA-ALD gels over MeHA-ALD gels (Figure S14, Supporting Information). Molecular weight was determined via size exclusion chromatography with multiangle light scattering (SEC-MALS). Original sodium hyaluronate and final product (RGD-MeHA-ALD) were dissolved at 0.3 mg mL^{-1} in phosphate-buffered saline (PBS) and heated to 95 °C to prevent aggregate formation, followed by elution through columns against MW standards (dextran) to obtain molecular weight profiles.

Biomaterial Application, Crosslinking, Penetrance, Retention:

For all in vitro studies, juvenile bovine trochlear cartilage was utilized (3–6 months old; Research 87), either as a disc (8 mm diameter × 100 μm) obtained by cryo-sectioning, or as a plug (8 mm diameter × 2.5 mm) by excision and cutting with parallel plates. For studies to evaluate the impact of aldehyde on HA attachment (Figure S3, Supporting Information), the modified HA (FITC-MeHA-ALD) was dissolved at 4 wt% (40 mg mL^{-1}) in PBS, and applied to juvenile bovine trochlear cartilage discs (8 mm diameter × 100 μm) for a specified duration of time (5, 10, 30 min), serially rinsed in PBS to remove nonadherent biomaterial, and imaged via fluorescent microscopy to quantify the degree of biomaterial attachment. To verify the cyto-compatibility of the biomaterial, cartilage plugs were sterilely dissected and subject to application of the HA therapy, PBS (positive), and 4% paraformaldehyde (PFA; negative control), cultured for 24 h, and stained with calcein-AM (live cells) and ethidium homodimer-1 (dead cells) to quantify percent viability (Live/Dead Cytotoxicity Kit; Life Technologies L3224).

For subsequent experiments on penetrance and retention, photoinitiator (Irgacure 2959; 0.05 wt%) was added to the HA solution to allow for UV light-induced polymerization. The modified HA solution (20 μL) was applied to cartilage plugs or discs for 5 min (unless otherwise specified) and crosslinked for 15 min (unless otherwise specified) with a light intensity of ≈5 mW cm^{-2} (320–400 nm). To obtain cross-sectional profiles for penetrance (after serial PBS rinses) and retention (after incubation in PBS at 37 °C for up to 7 d), cartilage plugs were fixed in PFA, embedded in optimal cutting temperature (OCT; Tissue-Tek) compound and frozen at −20 °C, cryo-sectioned to obtain 20 μm cross-sections, mounted with Prolong Gold with DAPI (to visualize cell nuclei), and imaged with an inverted fluorescent microscope.

Irradiance Measurements through Cartilage:

To measure UV light penetrance, 12 mm diameter cylindrical cartilage explants were excised from juvenile bovine trochlea using surgical biopsy punch. These plugs were set in OCT, frozen, and sectioned parallel to the articular surface at thicknesses ranging from 10 to 300 μm on a Leica cryostat. Samples were placed on glass microscope slides and hydrated in PBS. A UV lamp was positioned above a radiometer and set to an initial irradiance of ≈5 or 10 mW cm^{-2}, as measured through a glass slide. The aforementioned cartilage samples of varying thickness were placed between the radiometer and the UV lamp, such that the UV light had to pass through the sample before being detected by the radiometer sensor, and the resulting irradiance was measured (Figure S8, Supporting Information).

Multiscale Mechanical Testing:

To explore the effect of HA therapy on multiscale biphasic mechanics at the cartilage surface, both macro- and nanoindentation testing were performed. For macroscale testing, cylindrical cartilage plugs (8 mm diameter ×2.5 mm height) were excised from juvenile bovine femoral condyles, and cut using a freezing stage micro-tome to ensure flat and parallel surfaces, and so that the superficial zone was removed to mimic a focal defect (FD). A subset of plugs was digested surface-down in 350 μL of 0.1 wt% collagenase IV in serum-free Dulbecco's modified Eagle's medium (DMEM; Gibco) for 30 min at 37 °C to mimic degeneration (DD), followed by serial rinses in PBS and protease inhibitor (Sigma Aldrich; P2714). Samples were tested in uniaxial compression utilizing an Instron 5543 testing system and spherical indenter with a radius of 1 mm. Samples were preloaded to 0.05N, and strain was applied at approximately 1% s^{-1} until a load of 0.314 N was achieved; this load maintained for 30 min while measuring the creep deformation. Strain data as a function of time was fit with a Hertzian biphasic indentation model as described by Moore et al.[54] Output parameters of this model include compression modulus and permeability. After testing cartilage plugs without material, each sample was allowed to equilibrate in PBS for ≈2 h, followed by application of 15 μL of 4 wt% FITC-MeHA-Ald solution (with 0.05 wt% Irgacure 2959) for 5 minutes, UV crosslinking at approximately 5 mW cm^{-2} for 15 min (320–400 nm), serial rinses in PBS, and subsequent cartilage creep testing, as described above.

For nanoindentation testing, 8 mm diameter cartilage plugs were excised, as done with macro-scale testing, and sectioned to 100 μm thin cartilage discs to mimic focal defects (FD). A subset of discs was digested in 0.01 wt% collagenase to mimic degeneration (DD). Both FD and DD discs were mounted onto glass slides with a thin layer of super-glue adhesive, and hydrated for at least 60 min in PBS. Samples were indented using fiber-optical sensing probe with 10 μm radius spherical tip (Piuma Nanoindenter, Optics 11). Probe displacement was set to 5 μm, and the resulting force–indentation curves (up to 50% of max load) were fit to a Hertzian model to obtain a compressive modulus. Separate subsets of discs were also tested following HA therapy (15 μL for 5 min) and UV crosslinking (15 min, unless otherwise specified). At least four samples were tested per group, with 80–100 indentation points per sample (5 × 5 force maps, 4 maps per sample, 20 μm between indentation points).

In Vivo Study:

To assess the HA therapy in an in vivo articular setting, and to evaluate biomaterial retention, a pilot study was performed in three juvenile Yucatan minipigs (30–35 kg, 6–8 months old) under a protocol (#805077) approved by the Institutional Animal Care and Use Committee (IACUC) (805077). In a bilateral procedure, a medial patellar arthrotomy was performed to dislocate the patella laterally for access to the trochlear condyle. Four 4 mm diameter partial-thickness defects were created on each trochlea ($n = 6$ trochleas) by outlining the defect with a 4 mm biopsy punch and debriding the top of the defect with a surgical curette. Within each knee, each defect was randomly assigned to one of four conditions: empty defect (no HA therapy), HA therapy without crosslinking (+0), HA therapy with 5 min crosslinking (+5), and HA therapy with 15 min crosslinking (+15). For

the HA therapy, FITC-MeHA-ALD (15 μL) was applied to the top of each defect for 5 min, followed by crosslinking (320–400 nm, ≈5 mW cm^{-2}) for the specified time. Following sterile PBS rinses, the patella was repositioned, and the joint capsule, fascia, and skin were closed with sutures. Animals were euthanized at 7 d postoperatively, and stifle joints were recovered. Each individual defect was retrieved, fixed, and imaged on an inverted fluorescent microscope.

Chondrocyte Mechanotransduction Evaluation:

Live cartilage tissue was acquired from the trochleae of juvenile bovine stifle joints, within 24 h of slaughter, for both agarose construct and cartilage explant assays. For agarose construct assays, tissue was minced and digested in 0.01% collagenase overnight to release and isolate chondrocytes. Chondrocytes were expanded (Passage 1), encapsulated in 2% agarose gels (8 mm diameter ×2.5 mm height; 1 M cells mL^{-1}), and cultured in chondrogenic medium with TGF-β (10 ng mL^{-1}) for 3 d in order to promote pericellular matrix (PCM) formation. For cartilage explant assays, cartilage plugs (8 mm diameter) were cut to a thickness of 2.5 mm, removing both the superficial and calcified layers of cartilage. Explant plugs were cultured in basal media alone (Healthy; DMEM + 10% fetal bovine serum [FBS] + 1% penicillin—streptomycin-fungizone [PSF]) or basal media with 10ng/mL IL-1β (Degenerative) for 18 d. On the penultimate day of culture for both constructs and explants, modified HA (MeHA-ALD; 4 wt%; 20 μL) with photoinitiator (Irgacure 2959; 0.05 wt%) was applied to the top of constructs or explants and UV-crosslinked (320–400 nm, ≈5 mW cm^{-2} for 15 min), followed by culture for 24 h.

To evaluate calcium signaling, constructs and explants were incubated with a HEPES buffer solution containing 10×10^{-6} M Cal 520 AM (AAT Bioquest; Cat #21130), a calcium indicator, and pluronic acid (0.02 wt%) for 40 min. Samples were then placed in isotonic (≈330 mOsm) HEPES buffered media and imaged via confocal microscopy to obtain 12 min time series. Samples were then subject to an osmotic challenge by the addition of DI H_2O to obtain a hypotonic state (≈175 mOsm) and imaged again. Time-series, with visualization of calcium fluctuations, were processed to obtain mean fluorescence intensity versus time, the first derivative of which highlighted cellular response peaks.[27,44] These peaks were then used to determine the percentage of calcium-responsive cells.

MSC Culture Experiments:

To investigate MSC attachment, behavior, and response to cartilage tissue modified with HA therapy, MSCs were cultured on devitalized cartilage discs with and without treatment. For MSC isolation, juvenile bovine stifle joints were dissected, and cartilage surfaces were removed to expose the marrow elements. Bone marrow blocks were agitated in heparin-containing media (0.2 wt% heparin, 2% v/v PSF in sterile DMEM), and the resulting media/marrow mixture was plated and expanded. Passage 1 or Passage 2 MSCs were utilized from at least three individual donors for all MSC experiments. Devitalized cartilage samples for culture were obtained by excising the middle zone of bovine juvenile cartilage explants, and cryo-sectioning explants into 100 μm discs. Discs were sterilized, followed by rehydration with PBS. Similar to cartilage explant studies, and identical to nanoindentation studies, the modified HA (MeHA-ALD or RGD-MeHA-ALD; 15 μL) was applied to cartilage defects

for 5 min, and crosslinked (320–400 nm, ≈5 mW cm^{-2}) for 15 min (unless otherwise specified; Figures S15 and S16, Supporting Information). Discs were then serially rinsed in PBS to remove nonintegrated HA, placed in a 48-well non-TC treated plate, and seeded with MSCs. For focal adhesion (paxillin), mechano-sensation (YAP/TAZ), and pro-matrix synthesis phenotype (α-SMA) assays, discs were seeded with 500 cells in 500 μL of basal media. Focal adhesion and mechano-sensation experiments were retrieved at 24 h of culture, and promatrix phenotype experiments were retrieved at 7 d (with media replacement at day 1 and day 4).

MSC Immunostaining and Analysis:

For immunostaining of paxillin, cartilage discs seeded with cells were rinsed once in PBS, and underwent simultaneous fixation/permeabilization in microtubule stabilizing buffer (MTSB; 0.1 M PIPES, 1×10^{-3} M EGTA, 1×10^{-3} M $MgSO_4$, 4 wt% poly(ethylene glycol), 1.0% v/v Triton X-100, 2% paraformaldehyde) for 10 min, followed by serial PBS rinses, and primary and secondary antibodies for paxillin, and phalloidin to visualize the F-actin cytoskeleton. For immunostaining of YAP/TAZ and α-SMA, samples were rinsed once in PBS, fixed with 4% paraformaldehyde for 20 min, rinsed 3× with PBS, permeabilized (0.5% Triton-X-100, 316×10^{-3} M sucrose, 7.14×10^{-3} M $MgCl_2$ in PBS), rinsed 3× with PBS, and stained with primary and secondary antibodies for YAP/TAZ and phalloidin (Table 1). All samples mounted between two glass coverslips with ProLong Gold with DAPI and were imaged via confocal microscopy to obtain z-stack images. For focal adhesion (FA) analysis, a z-stack projection with sum of slices yielded 2D images of FAs, which were analyzed via the UNC Focal Adhesion Analysis Server (Threshold = 3.0) to obtain FA number and total FA area per cell. To obtain cell area, the F-actin channel z-stack was converted to a maximum intensity projection and binarized through a Huang filter, and the binary image was used to obtain cell area. For YAP/TAZ nuclear, a maximum intensity projection of the YAP/TAZ channel was overlaid with the nucleus (DAPI channel), and the signal intensities within and immediately around the nucleus were measured.

Metabolic Labeling for Nascent Matrix—Culture, Staining, Analysis:

For metabolic labeling to visualize nascent matrix deposition, high glucose DMEM without glutamine, methionine, or cysteine (ThermoFisher: Cat# 21013024) was supplemented with 10% FBS and 1% PSF, gluta-max (2×10^{-3} M), L-cystine (0.2×10^{-3} M), sodium pyruvate (100 μg mL^{-1}), AHA (75×10^{-6} M; Click Chemistry Tools, Cat #1066), L-methionine (25×10^{-6} M). A 75/25 ratio of AHA to L-methionine was chosen to still allow for sufficient visualization while maintaining cell viability and activity. Media was replaced with fresh AHA-containing media on days 1, 3, and 5, and cultures were terminated on day 7. Samples were then washed twice in PBS with 3% bovine serum albumin (BSA), stained with DBCO-555 (Click Chemistry Tools, Cat #1290, 30 μm) for 30 min at 37 °C, rinsed 3× in PBS, fixed in 4% PFA, rinsed 3× in PBS, and mounted with ProLong Gold with DAPI. Confocal z-stack images were taken and maximum intensity projections were binarized to calculate percent matrix coverage.

Statistical Analysis:

Results were presented according to number of data points, as a dot plot, dot plot with bar graph (mean ± standard deviation), or violin plot (median and quartiles presented). For dot plots, paired replicates are joined by a connecting line. Statistical analyses were performed with GraphPad Prism 8 for Windows. To analyze all data sets, outliers were first removed with a robust regression and outlier removal (ROUT) method, followed by testing for normality with a D'Agostino-Pearson test. For comparing two populations, a two-tailed student's t-test was used for normally distributed data, a Mann-Whitney U-test was performed for non-normal or nonparametric data, and paired tests were performed for replicate data. Statistical testing of datasets with more than two populations involved one-way analysis of variance (ANOVA) with post-hoc Tukey's multiple comparisons tests on normal distributions or a Kruskal-Wallis test with post-hoc Dunn's multiple comparisons test for non-normal data. Statistical significance was indicated by *, **, ***, and ****, representing $p < 0.05$, 0.01, 0.001, and 0.0001, respectively.

Data Availability Statement

The data that support the findings of this study are available from the corresponding author upon reasonable request.

Supplementary Material

Refer to Web version on PubMed Central for supplementary material.

Acknowledgements

The authors acknowledge Anthony Martin for his assistance in initial biomaterial development, Daphney Chery and Lin Han for their assistance in chondrocyte mechano-response assays, and Hannah Zlotnick for her assistance in the in vivo studies. This work was supported by the National Institutes of Health (R01 AR056624), the National Science Foundation Center for Engineering Mechanobiology (CMMI-1548571), the Department of Veterans Affairs (IK1 RX003208 and IK6 RX003416), the Penn Center for Musculoskeletal Disorders (P30 AR069619), and Penn Health Tech (Medical Devices and Health Technology Development Project).

References

[1]. Sophia Fox AJ, Bedi A, Rodeo SA, Sports Health 2009, 1, 461. [PubMed: 23015907]

[2]. Soltz MA, Ateshian GA, Ann. Biomed. Eng 2000, 28, 150. [PubMed: 10710186]

[3]. Park S, Krishnan R, Nicoll SB, Ateshian GA,J. Biomech 2003, 36, 1785. [PubMed: 14614932]

[4]. Ateshian GA,J. Biomech 2009, 42, 1163. [PubMed: 19464689]

[5]. Venäläinen MS, Mononen ME, Salo J, Räsänen LP, Jurvelin JS, Töyräs J, Virén T, Korhonen RK, Sci. Rep 2016, 6, 37538. [PubMed: 27897156]

[6]. Bonassar LJ, Grodzinsky AJ, Srinivasan A, Davila SG, Trippel SB, Arch. Biochem. Biophys 2000, 379, 57. [PubMed: 10864441]

[7]. Guilak F, Best Pract. Res., Clin. Rheumatol 2011, 25, 815. [PubMed: 22265263]

[8]. June RK, Fyhrie DP, Biomed. Eng. Online 2009, 8, 32. [PubMed: 19889234]

[9]. Griffin DJ, Vicari J, Buckley MR, Silverberg JL, Cohen I, Bonassar LJ,J. Orthop. Res 2014, 32, 1652. [PubMed: 25196502]

[10]. Basalo IM, Nauck RL, Kelly TA, Nicoll SB, Chen FH, Hung CT, Ateshian GA,J. Biomech. Eng 2004, 126, 779. [PubMed: 15796336]

[11]. Grenier S, Donnelly PE, Gittens J, Torzilli PA, J. Biomech. 2015, 48, 122. [PubMed: 25468298]

[12]. Peters AE, Akhtar R, Comerford EJ, Bates KT, Sci. Rep 2018, 8, 5931. [PubMed: 29651151]
[13]. Hjelle K, Solheim E, Strand T, Muri R, Brittberg M, Arthroscopy 2002, 18, 730. [PubMed: 12209430]
[14]. Martín AR, Patel JM, Zlotnick HM, Carey JL, Mauck RL, npj Regener. Med 2019, 4, 12.
[15]. Gracitelli GC, Moraes VY, Franciozi CES, Luzo MV,Belloti JC, Cochrane Database Syst. Rev 2016, 9, CD010675. [PubMed: 27590275]
[16]. Solheim E, Hegna J, Inderhaug E, Øyen J, Harlem T, Strand T, Knee Surg., Sports Traumatol. Arthrosc 2016, 24, 1587. [PubMed: 25416965]
[17]. Mäkelä JTA, Cooper BG, Korhonen RK, Grinstaff MW, Snyder BD, Osteoarthritis Cartilage 2018, 26, 414. [PubMed: 29326062]
[18]. Bonitsky CM, McGann ME, Selep MJ, Ovaert TC, Trippel SB, Wagner DR, J. Orthop. Res 2017, 35, 558. [PubMed: 27584857]
[19]. Patel JM, Saleh KS, Burdick JA, Mauck RL, Acta Biomater. 2019, 93, 222. [PubMed: 30711660]
[20]. Cosgrove BD, Mui KL, Driscoll TP, Caliari SR, Mehta KD, Assoian RK, Burdick JA, Mauck RL, Nat. Mater 2016, 15, 1297. [PubMed: 27525568]
[21]. Caliari SR, Vega SL, Kwon M, Soulas EM, Burdick JA, Biomaterials 2016, 103, 314. [PubMed: 27429252]
[22]. Mardones R, Jofré CM, Tobar L, Minguell JJ, J. Hip Preserv. Surg 2017, 4, 159. [PubMed: 28630737]
[23]. Mehrabani D, Mojtahed Jaberi F, Zakerinia M, Hadianfard MJ, Jalli R, Tanideh N, Zare S, World J. Plast. Surg 2016, 5, 168. [PubMed: 27579273]
[24]. Murphy JM, Fink DJ, Hunziker EB, Barry FP, Arthritis Rheumatol. 2003, 48, 3464.
[25]. Fisher MB, Belkin NS, Milby AH, Henning EA, Bostrom M, Kim M, Pfeifer C, Meloni G, Dodge GR, Burdick JA, Schaer TP, Steinberg DR, Mauck RL, Tissue Eng., Part A 2015, 21, 850. [PubMed: 25318414]
[26]. Setton LA, Elliott DM, Mow VC, Osteoarthritis Cartilage 1999, 7, 2. [PubMed: 10367011]
[27]. Chery DR, Han B, Li Q, Zhou Y, Heo S-J, Kwok B, Chandrasekaran P, Wang C, Qin L, Lu XL, Kong D, Enomoto-Iwamoto M, Mauck RL, Han L, Acta Biomater. 2020, 111, 267. [PubMed: 32428685]
[28]. Guilak F, Nims RJ, Dicks A, Wu CL, Meulenbelt I, Matrix Biol. 2018, 71, 40. [PubMed: 29800616]
[29]. Owen JR, Wayne JS, Biomech. Model. Mechanobiol 2006, 5, 102. [PubMed: 16506018]
[30]. Sanchez-Adams J, Leddy HA, McNulty AL, O'Conor CJ, Guilak F, Curr. Rheumatol. Rep 2014, 16, 451. [PubMed: 25182679]
[31]. Chan DD, Cai L, Butz KD, Trippel SB, Nauman EA, Neu CP, Sci. Rep 2016, 6, 19220. [PubMed: 26752228]
[32]. Strauss EJ, Hart JA, Miller MD, Altman RD, Rosen JE, Am. J. Sports Med 2009, 37, 1636. [PubMed: 19168804]
[33]. Burdick JA, Prestwich GD, Adv. Mater 2011, 23, H41. [PubMed: 21394792]
[34]. Burdick JA, Chung C, Jia X, Randolph MA, Langer R, Biomacro-molecules 2005, 6, 386.
[35]. Wang D-A, Varghese S, Sharma B, Strehin I, Fermanian S, Gorham J, Fairbrother DH, Cascio B, Elisseeff JH, Nat. Mater 2007, 6, 385. [PubMed: 17435762]
[36]. Hall AC, Curr. Rheumatol. Rep 2019, 21, 38. [PubMed: 31203465]
[37]. Zhou Y, David MA, Chen X, Wan LQ, Duncan RL, Wang L, Lu XL, Ann. Biomed. Eng 2016, 44, 1138. [PubMed: 26219403]
[38]. Zelenski NA, Leddy HA, Sanchez-Adams J, Zhang J, Bonaldo P, Liedtke W, Guilak F, Arthritis Rheumatol. 2015, 67, 1286. [PubMed: 25604429]
[39]. Dall'Oca C, Breda S, Elena N, Valentini R, Samaila EM, Magnan B, Acta Biomed. 2019, 90, 75.
[40]. Lee W-S, Kim HJ, Kim K-I, Kim GB, Jin W, Stem Cells Transl. Med 2019, 8, 504. [PubMed: 30835956]
[41]. Kim Y, Kumar S, Mol. Cancer Res 2014, 12, 1416. [PubMed: 24962319]

[42]. Kim IL, Khetan S, Baker BM, Chen CS, Burdick JA, Biomaterials 2013, 34, 5571. [PubMed: 23623322]

[43]. Dupont S, Morsut L, Aragona M, Enzo E, Giulitti S, Cordenonsi M, Zanconato F, Digabel JL, Forcato M, Bicciato S, Elvassore N, Piccolo S, Nature 2011, 474, 179. [PubMed: 21654799]

[44]. Bonnevie ED, Gullbrand SE, Ashinsky BG, Tsinman TK, Elliott DM, Chao P.-h. G., Smith HE, Mauck RL, Nat. Biomed. Eng 2019, 3, 998. [PubMed: 31611678]

[45]. Liu F, Lagares D, Choi KM, Stopfer L, Marinković A, Vrbanac V, Probst CK, Hiemer SE, Sisson TH, Horowitz JC, Rosas IO, Fredenburgh LE, Feghali-Bostwick C, Varelas X, Tager AM, Tschumperlin DJ, Am. J. Physiol.: Lung Cell. Mol. Physiol 2015, 308, L344. [PubMed: 25502501]

[46]. Talele NP, Fradette J, Davies JE, Kapus A, Hinz B, Stem Cell Rep. 2015, 4, 1016.

[47]. Loebel C, Mauck RL, Burdick JA, Nat. Mater 2019, 18, 883. [PubMed: 30886401]

[48]. Mcleod CM, Mauck RL, Sci. Rep 2016, 6, 38852. [PubMed: 27941914]

[49]. Lim KS, Klotz BJ, Lindberg GCJ, Melchels FPW, Hooper GJ, Malda J, Gawlitta D, Woodfield TBF, Macromol. Biosci 2019, 19, 1900098.

[50]. Maas SA, Ellis BJ, Ateshian GA, Weiss JA, J. Biomech. Eng 2012, 134, 011005. [PubMed: 22482660]

[51]. Ateshian GA, Warden WH, Kim JJ, Grelsamer RP, Mow VC, J. Biomech 1997, 30, 1157. [PubMed: 9456384]

[52]. Guo H, Maher SA, Torzilli PA,J. Biomech 2015, 48, 166. [PubMed: 25465194]

[53]. Loebel C, Rodell CB, Chen MH, Burdick JA, Nat. Protoc 2017, 12, 1521. [PubMed: 28683063]

[54]. Moore AC, DeLucca JF, Elliott DM, Burris DL, J. Tribol 2016, 138, 414051.

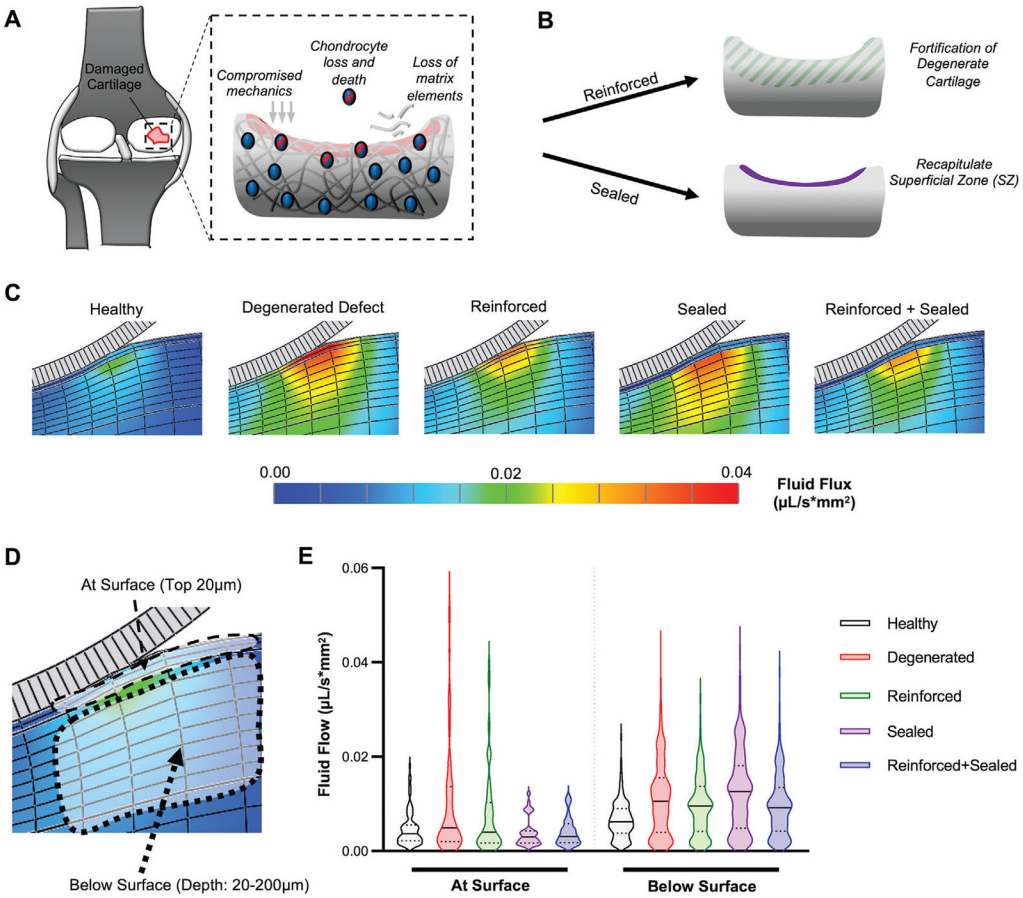

Figure 1.

Cartilage stabilization via a combination of reinforcement and sealing. A) Schematic depicting the consequences of cartilage injury, including compromised mechanics, chondrocyte death, and matrix loss. B) Two approaches to stabilize damaged cartilage: biomaterial-mediated (BM) reinforcement and superficial-zone (SZ) like sealing. C) Finite element simulation of fluid flux (μL/s*mm^2) in different scenarios: Healthy cartilage with intact superficial zone, degenerated defect, reinforced degenerated defect, sealed degenerated defect, and reinforced and sealed degenerated defect. Color bar range = 0.00–0.04. D) Schematic depicting cartilage at surface (top 20 μm) and below surface (20–200 μm). E) Distribution of fluid flux (μL/s*mm^2) either at or below surface. Single distribution is represented as violin plot.

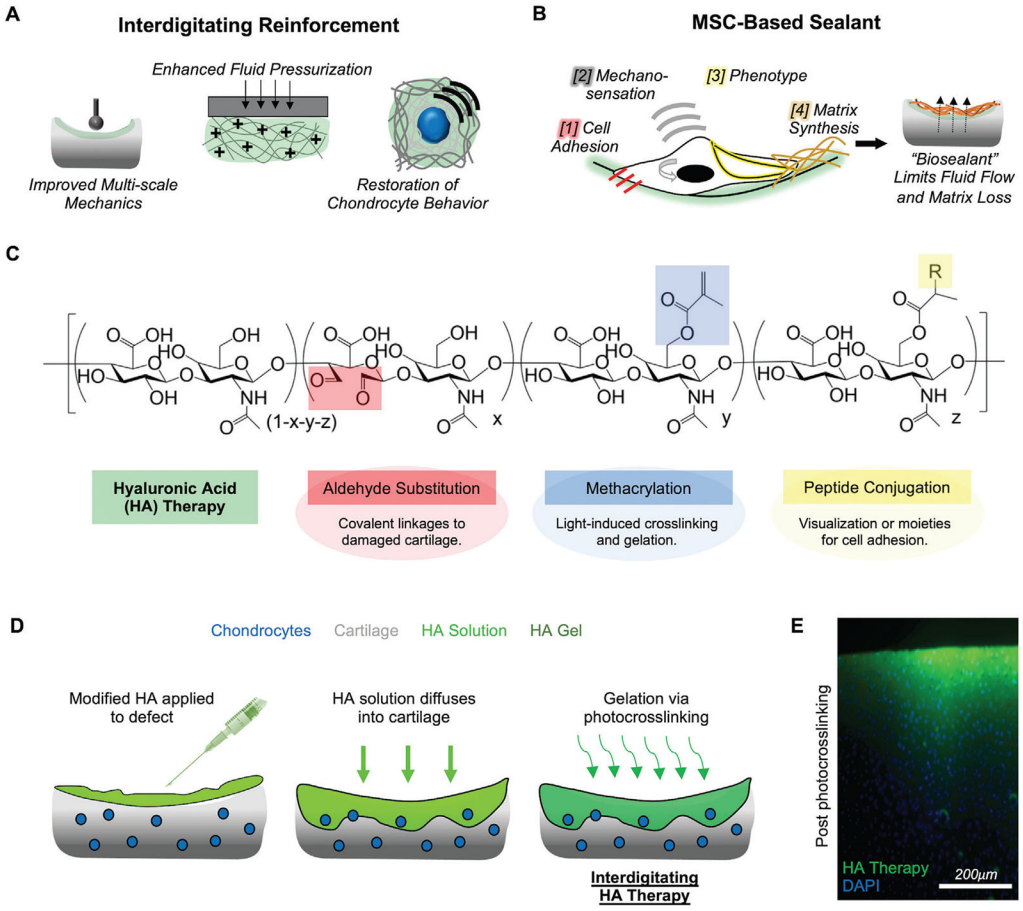

Figure 2.

Hyaluronic acid therapy designed to reinforce and seal damaged cartilage. A) Interdigitating microenvironment provides improved multiscale mechanics, enhances fluid pressurization, and restores chondrocyte behavior. B) Living MSC-based barrier is created through 1] cell adhesion, 2] mechano-sensation, 3] promatrix phenotype, and 4] matrix synthesis and deposition, to create a “sealant” that could limit fluid flow and matrix loss. C) Hyaluronic acid (HA) is modified for functional application in this study; aldehyde substitution promotes linkage to damaged tissue, methacrylation permits light-induced gelation, and peptide conjugation allows for visualization and control of cell adhesion. D) HA solution is applied to cartilage defects, allowed to diffuse in, and is crosslinked into place to form an interdigitating microenvironment. E) Cross-section of cartilage tissue (cell nuclei in blue; DAPI) with fluorescein-conjugated HA therapy (green; applied for 5 min), post photocrosslinking (320–400 nm, ≈5mW cm^{-2}, 15 min). Scale bar = 200 μm.

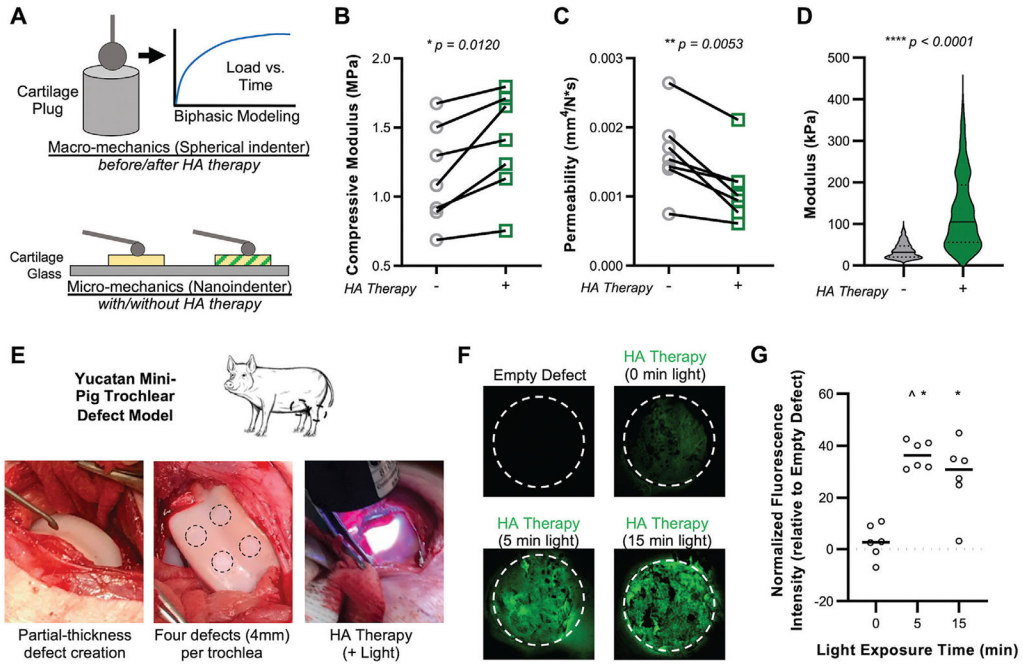

Figure 3.

Interdigitating HA therapy improves multi-scale biomechanics and is retained at the defect site. A) Fortified cartilage was evaluated mechanically by macro-scale creep indentation testing (for biphasic properties), and by nanoindentation for cell-scale mechanical properties. B) Macroscale compressive modulus and C) permeability of degenerated cartilage tissue (digested in 0.01% collagenase type IV for 30 min) before (−) and after (+) HA therapy (5 min application; 15 min crosslinking, 320–400 nm, ≈5 mW cm^{-2}). $n = 7$ paired samples. D) Microscale modulus measured by nanoindentation in degenerated cartilage before (−) and after (+) HA therapy. $n > 400$ measurements ($n = 5$ specimens per group). E) HA solution applied and crosslinked in trochlear defects in a Yucatan mini-pig model. F) HA therapy was retained in cartilage defects at 7 d with both 5 and 15 min of light exposure (crosslinking). White dashed line outlines defect. G) Normalized fluorescence intensity in defects, relative to empty defect controls. * and ^ depict $p < 0.05$ versus empty defect and +0. $n = 6$ defects per group, normalized to empty defect within the same knee. Horizontal line depicts mean.

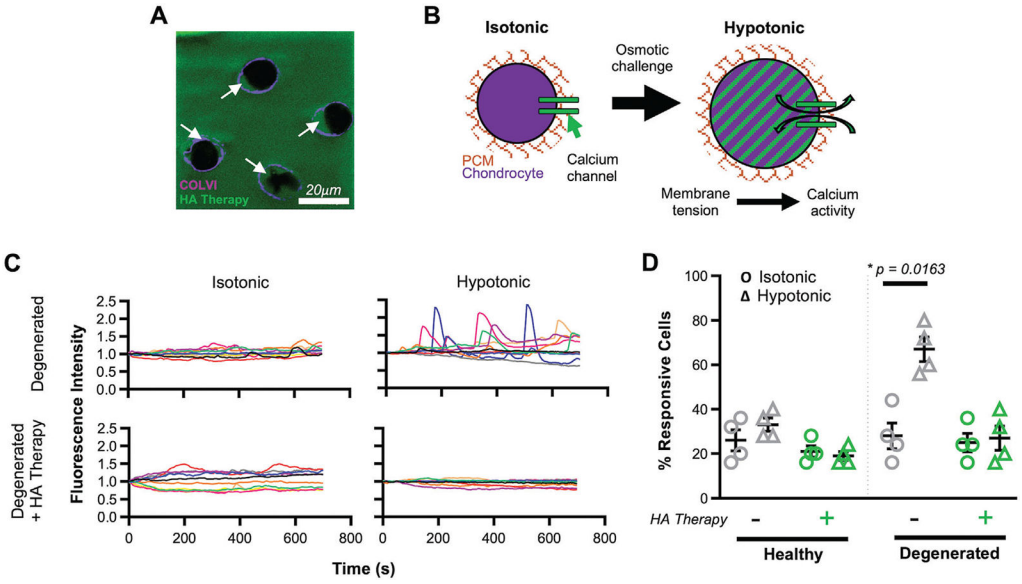

Figure 4.

HA therapy restores chondrocyte mechanotransduction. A) Visualization of HA therapy (green) around chondrocytes (black voids) and within the pericellular matrix (PCM; depicted by collagen type VI in magenta; highlighted by white arrows). B) Schematic showing the increase in membrane tension and calcium signaling in chondrocytes under osmotic challenge. C) Sample traces ($n = 10$) of calcium flux in chondrocytes within cartilage explants overtime. Degenerated cartilage (culture with 10 ng mL^{-1} IL-1β) with and without HA therapy are shown, in isotonic and hypotonic conditions. D) % of calcium-responsive chondrocytes in healthy and degenerated cartilage with and without HA therapy. Isotonic (O) and hypotonic (Δ) conditions are shown. mean ± standard deviation. $n = 4$ biological replicates, $n > 100$ cells per replicate. * indicates $p < 0.05$.

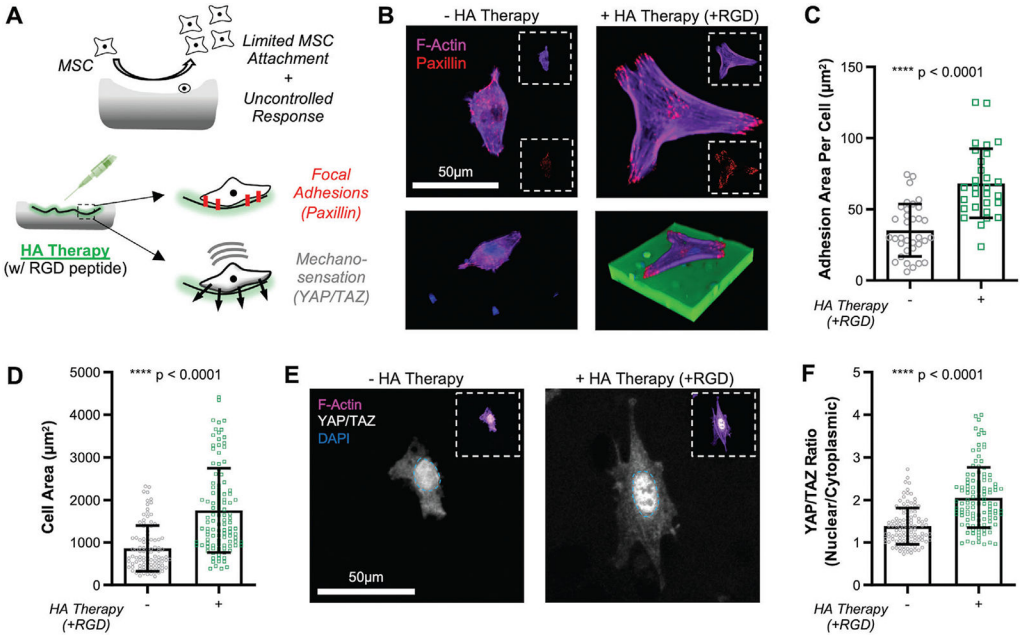

Figure 5.

HA therapy of degenerated cartilage improves MSC attachment and mechanosensation. A) Schematic depicting how HA therapy (with RGD peptide) can improve focal adhesions (visualized via paxillin) and mechanosensation (YAP/TAZ). B) F-actin (magenta) and paxillin (red) staining of MSCs cultured (t = 24 h) on degenerated cartilage alone with and without cartilage modification by HA therapy (+RGD). Insets show individual channels. Scale bar = 50 μm. (Bottom) 3D rendering of attached cell, included nuclear staining (DAPI; blue) and HA (FITC; green). C) Adhesion area per cell (via paxillin) on degenerated cartilage with and without HA therapy (+RGD). mean ± standard deviation, n > 30 cells per group, from three biological replicates. D) Cell area on degenerated cartilage with and without HA therapy (+RGD). mean ± standard deviation, n > 100 cells per group, from three biological replicates. E) YAP/TAZ (white) of cells cultured (t = 24 h) on degenerated cartilage with and without HA therapy (+RGD). Nucleus border depicted with blue dashed line. Inset shows individual channels [F-actin (magenta), DAPI (blue), YAP/TAZ (white)]. Scale bar = 50 μm. F) YAP/TAZ nuclear localization, measured by the ratio of intensity in the nucleus to that in the cytoplasm, for MSCs on control and modified cartilage. mean ± standard deviation, n > 60 cells per group, from three biological replicates.

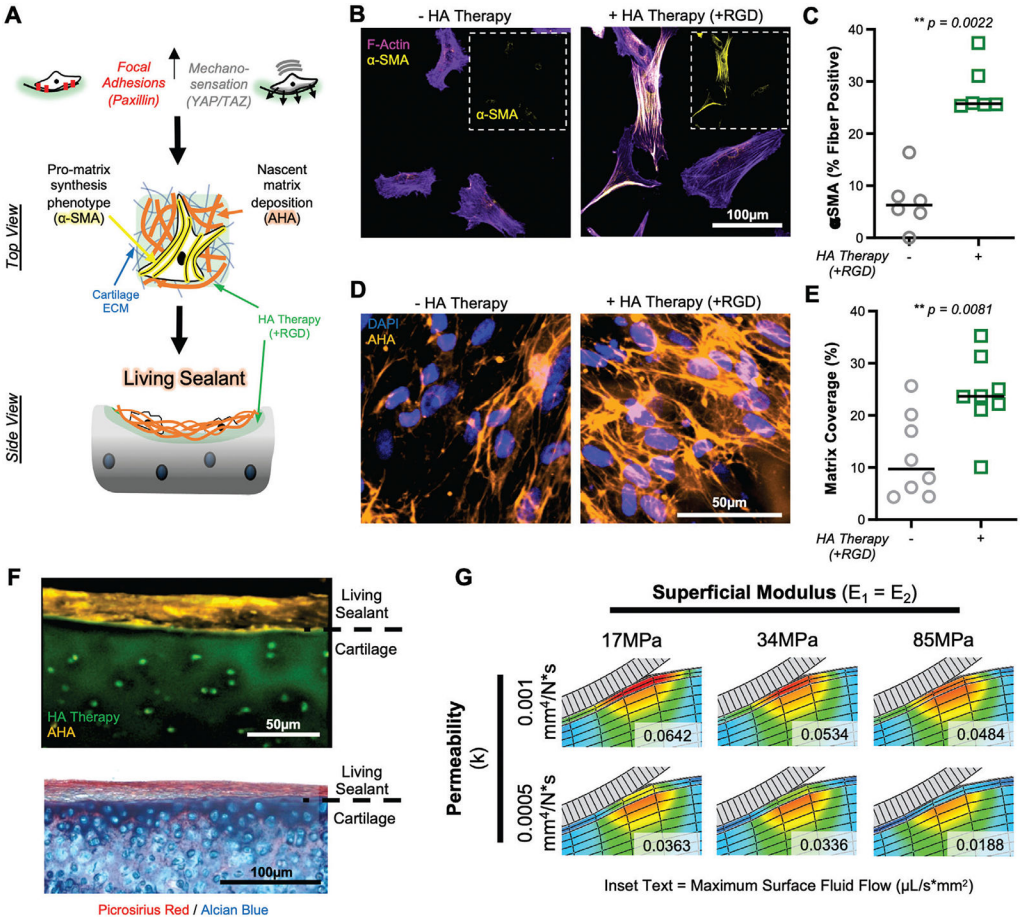

Figure 6.

HA therapy promotes MSC-guided matrix synthesis on degenerated cartilage tissue. A) Schematic depicting how adhesion and mechanosensation drive α-smooth muscle actin (α-SMA) positive stress fiber formation and deposition of nascent matrix, to form a living sealant on damaged cartilage. B) F-actin (magenta) and α-SMA (yellow) staining of MSCs cultured (t = 7 d) on degenerated cartilage with and without HA therapy (+RGD). Inset shows α-SMA channel alone. Scale bar = 100 μm. C) Percent of cells positive for α-SMA stress fibers. n = 6 replicates per group, n > 30 cells per group per replicate. D) Nascent matrix deposition, visualized by staining of azidohomoalanine (AHA; orange), on cartilage with and without HA therapy (+RGD) after 7 d of culture. Scale bar = 50 μm. E) Percent of cartilage area covered by nascent matrix. n = 7 replicates, n = 5 images per replicate. F) Top: Cross-sectional view of nascent matrix (orange) covering the surface of cartilage explant treated with HA therapy (green). Bottom: Histological image of cartilage explant with HA therapy, seeded with MSCs, and cultured for 7 d, showing the formation of a living barrier. Collagenous (picrosirius red) and glycosaminoglycan (Alcian blue) visualized. G) Finite element modeling of orthotropic sealant layer showing impact of sealant permeability and tensile modulus ($E_1 = E_2$, both parallel to articular surface) on fluid flux (μL/s*mm^2) at the cartilage surface. Inset text represents maximum fluid flow at the cartilage surface (top 20 μm).

Table 1.

Primary and secondary antibodies, and immunostaining, used in this study, with product number, vendor, specific lot number, and dilution.

Antibody	Product #	Vendor	Lot#	Dilution
YAP (mouse monoclonal)	SC-101199	Santa Cruz Biotechnology	LO216	1:200
Paxillin (purified mouse antipaxillin)	610052	BD Biosciences	7201859	1:500
αSMA (mouse monoclonal)	A2547	Sigma Aldrich	076M4784V	1:200
Fibronectin (mouse monoclonal)	F6140	Sigma Aldrich	057M4780V	1:200
AlexaFluor 555 goat antimouse IgG (H+L)	A21424	Invitrogen	1892094A, 1975522	1:200
AlexaFluor 555 DBCO	1290	Click Chemistry Tools	N/A	1:200 (30×10^{-6} M)
AlexaFluor 647 Phalloidin	A22287	Invitrogen	1941485, 2053477	1:100
ProLong Gold antifade reagent with DAPI	P36935	Invitrogen	2019932, 2069602	1 drop